Neural Network-Based Stator Current Control for Rated Power Regulation of Permanent Magnet Synchronous Generator Wind Turbines with Differential Evolution Pitch Optimization

Hazem Hassan Ali Sayed
Energy Management Department, Luminous Energy Solutions, Calgary, Canada
Renewable Energy Department, New Cairo Technological University, Egypt

Abstract. The main objective of this study is to achieve precise regulation of the Machine Side Converter (MSC) stator quadrature-axis current in a Permanent Magnet Synchronous Generator (PMSG) wind turbine, in order to reach rated maximum power at wind speeds exceeding the rated limit while preventing excessive current surges that could damage converter components, since a comprehensive comparison between adaptive Neural Network (NN) and Proportional Integral (PI) controllers for this purpose remains insufficiently addressed in the literature. These objectives were achieved by solving the following tasks: an accurate pitch angle estimation method was developed for wind speeds exceeding the rated value using the Differential Evolution (DE) algorithm; a PI controller was tuned to maintain the PMSG electrical angular speed at its rated value through the DE-optimized pitch angles; an adaptive NN controller, trained online using online delta-rule backpropagation algorithm, was developed to directly regulate the MSC stator quadrature-axis current; and both control schemes were implemented in MATLAB/Simulink under variable wind speed and generator inertia conditions. The most important results are that the MSC-based NN controller achieved rated maximum power with zero overshoot, compared to 72.9% overshoot in active power obtained with the PI-based speed regulator, and markedly reduced overshoots in the stator current, mechanical torque, rotor speed, and DC-link voltage. The significance of the obtained results lies in showing that direct neural-network-based current regulation protects MSC components from excessive current stress, extends system lifespan, and offers a scalable solution for large-scale wind energy deployment.
Keywords: online delta-rule backpropagation algorithm, stator quadrature-axis current, rated power regulation, evolutionary optimization, variable speed wind turbine.

DOI: https://doi.org/10.52254/1857-0070.2026.3-71.01
UDC: 621.3: 681.5

Controlul curentului statoric bazat pe rețele neuronale pentru controlul puterii nominale a turbinelor eoliene cu generatoare sincrone cu magneți permanenți și optimizarea unghisului de pas al palelor prin metoda evoluției diferențiale

Hazem Hassan Ali Sayed
Departamentul de Management Energetic, Luminous Energy Solutions, Calgary, Canada
Departamentul de Energie Regenerabilă, Universitatea Tehnologică din New Cairo, Egipt
Rezumat. Obiectivul principal al acestui studiu este realizarea unei reglări precise a curentului în cuadratură al statorului Convertorului de pe Partea Mașinii (Machine-Side Converter – MSC) într-o turbină eoliană cu generator sincron cu magneți permanenți (PMSG), pentru a atinge puterea maximă nominală la viteze ale vântului care depășesc valoarea nominală, prevenind, în același timp, supracurenții care ar putea deteriora componentele convertorului, deoarece o comparație cuprinzătoare între regulatoarele adaptive bazate pe Rețele Neuronale (NN) și cele Proporțional-Integrale (PI) pentru acest scop rămâne insuficient abordată în literatura de specialitate. Aceste obiective au fost atinse prin rezolvarea următoarelor sarcini: a fost dezvoltată o metodă precisă de estimare a unghiului de pas pentru viteze ale vântului care depășesc valoarea nominală, utilizând algoritmul evoluție diferențială (DE); a fost reglat un regulator PI pentru a menține viteza unghiulară electrică a PMSG la valoarea nominală prin utilizarea unghiurilor de pas optimizate cu algoritmul DE; a fost dezvoltat un regulator adaptiv bazat pe o rețea neuronală (NN), antrenat online utilizând algoritmul de retropropagare online bazat pe regula delta, pentru a regla direct curentul în cuadratură al statorului MSC; iar ambele scheme de control au fost implementate în MATLAB/Simulink în condiții de viteză variabilă a vântului și de variație a inerției generatorului. Cele mai importante rezultate arată că regulatorul NN bazat pe MSC a atins puterea maximă nominală fără depășire,

comparativ cu depășirea de 72.9 % a puterii active obținută în cazul regulatorului de viteză bazat pe PI, precum și o reducere semnificativă a depășirilor curentului statoric, cuplului mecanic, vitezei rotorului și tensiunii din circuitul de curent continuu. Semnificația rezultatelor obținute constă în demonstrarea faptului că reglarea directă a curentului, bazată pe o rețea neuronală, protejează componentele MSC împotriva solicitărilor excesive de curent, prelungește durata de viață a sistemului și oferă o soluție scalabilă pentru implementarea energiei eoliene la scară largă.
Cuvinte-cheie: algoritm online de retropropagare cu regula delta, curent statoric în cuadratură, reglare a puterii nominale, optimizare evolutivă, turbină eoliană cu viteză variabilă.

Управление током статора для регулирования номинальной мощности ветровых турбин с синхронными генераторами с постоянными магнитами на основе нейронной сети с оптимизацией угла наклона лопастей методом дифференциальной эволюции

Хазем Хассан Али Сайед
Отдел управления энергопотреблением, Luminous Energy Solutions, Калгари, Канада
Отдел возобновляемых источников энергии, Технологический университет Нового Каира, Египет
Аннотация. Основная цель данного исследования — достижение точного регулирования тока по квадратурной оси статора преобразователя со стороны машины (ПСМ) в ветротурбине с синхронным генератором с постоянными магнитами (ГПМ) для достижения номинальной максимальной мощности при скоростях ветра, превышающих номинальный предел, и предотвращения чрезмерных скачков тока, которые могут повредить компоненты преобразователя, поскольку всестороннее сравнение адаптивных нейронных сетей (НС) и пропорционально-интегральных (ПИ) регуляторов для этой цели недостаточно освещено в литературе. Эти цели были достигнуты путем решения следующих задач: разработан точный метод оценки угла наклона лопастей для скоростей ветра, превышающих номинальное значение, с использованием алгоритма дифференциальной эволюции (ДЭ); настроен ПИ-регулятор для поддержания электрической угловой скорости ГПМ на номинальном значении за счет оптимизированных с помощью ДЭ углов наклона лопастей; разработан адаптивный нейронный-регулятор, обученный в режиме онлайн с использованием алгоритма обратного распространения ошибки дельта-правила, для непосредственного регулирования тока по квадратурной оси статора ПСМ; и обе схемы управления были реализованы в Матлаб/Симулинк в условиях переменной скорости ветра и инерции генератора. Наиболее важными результатами являются то, что контроллер на основе нейронной сети с использованием ПСМ достиг номинальной максимальной мощности без перерегулирования, по сравнению с перерегулированием активной мощности в 72.9%, полученным с помощью регулятора скорости на основе ПИ-регулятора, и значительно снизил перерегулирование тока статора, механического крутящего момента, скорости вращения ротора и напряжения звена постоянного тока. Значимость полученных результатов заключается в демонстрации того, что прямое регулирование тока на основе нейронной сети защищает компоненты ПСМ от чрезмерной токовой нагрузки, продлевает срок службы системы и предлагает масштабируемое решение для крупномасштабного развертывания ветроэнергетических установок.
Ключевые слова: онлайн-алгоритм обратного распространения ошибки по правилу дельта, ток по квадратурной оси статора, регулирование номинальной мощности, эволюционная оптимизация, ветровая турбина с переменной скоростью вращения.

INTRODUCTION

Wind energy has become one of the most rapidly growing renewable energy sources worldwide, driven by the urgent need to reduce dependence on fossil fuels and mitigate climate change impacts. The Permanent Magnet Synchronous Generator (PMSG) has emerged as the predominant wind turbine type among pitch-adjusting variable-speed systems due to its high efficiency, reliability, and elimination of external excitation requirements [1]-[3]. Utilizing a PMSG-based Wind Energy Conversion System (WECS) with a Zero d-Axis Current (ZDPC) control scheme, applied as part of Field-Oriented Control (FOC), enables the generation of rated output power across wind speeds from rated to cut-out levels.

This is achieved by maintaining a constant rotor speed at the rated value through control of the stator quadrature-axis current of the Machine Side Converter (MSC), effectively capping the wind turbine power output at the rated level [4]-[5].

Inaccurate pitch angle and stator quadrature-axis current values for the wind turbine blades and MSC circuit can lead to critical issues including failure to reach the wind turbine rated power limitation, triggering alarms in PMSG wind turbines where error pitch activation causes the turbine to stop and waste energy, and damaging the generator at high wind speeds [6]-[7]. As a result, the pitch mechanism control system based on stator quadrature-axis current, which uses either hydraulic or electric pitch actuators, is crucial to this process [8]-[9]. The main challenge is to reduce excessive stress on the generator and power converter components during pitch control mode, requiring precise optimization of power generation to minimize power increases above rated value.

Considerable research has addressed pitch control systems in PMSG wind turbines. Several studies have focused on conventional Proportional Integral (PI) controllers for pitch angle regulation [10]-[11]. In [12], pitch angle optimization for small wind turbines was presented using a teaching-learning-based optimization algorithm, though the importance of Machine Side Converter current in pitch control was neglected.

Adaptive pitch control for variable-pitch PMSG wind turbines was explored in [13], but findings only confirmed the use of conventional controllers without addressing reference value estimation for pitch control mode. A comparison of different pitch controllers in wind farms was conducted in [14], relying solely on conventional PI controller methods without quantifying output power accuracy. Nonlinear PI control for variable-pitch wind turbines was proposed in [15], but failed to account for all system electrical dynamics under disturbances. Proportional Integral controllers with Particle Swarm Optimization were used in [16] to adjust controller gains, while a PID control model with Differential Evolution optimization was designed in [17] for gain scheduling.

An Artificial Neural Network adapter for automatic PID parameter regulation was introduced in [18], employing improved gradient descent to optimize network weights.

Despite these contributions, significant gaps remain in the existing literature. First, no comprehensive comparison between adaptive Neural Network and PI controllers specifically targeting MSC stator quadrature-axis current regulation under optimal pitch angle estimation has been reported. Second, the combined effect of Differential Evolution-based pitch angle optimization with direct Neural Network current control for protecting MSC components from excessive current overshoots remains insufficiently addressed. Third, most existing studies use unrealistic wind speed profiles and neglect the impact of generator inertia variations on controller performance. These gaps represent the primary motivation for this work.

To tackle these issues, this study employs the Differential Evolution optimization method to solve the one-variable nonlinear equation governing the pitch angle. The proposed approach involves two key steps: deriving a wind speed-pitch angle curve input/output relationship using Differential Evolution, and utilizing both Neural Network and Proportional Integral controllers within the MSC circuit. The Neural Network controller, utilizing online delta-rule backpropagation algorithm, directly regulates the stator MSC quadrature-axis current, while the PI controller maintains the electrical angular speed at the PMSG rated value through optimal pitch angles obtained via Differential Evolution. The main contributions of this work are: (1) accurate pitch angle estimation using Differential Evolution for wind speeds exceeding the rated value; (2) evaluation of PI controller gains in the MSC circuit for stator quadrature-axis current control; (3) application of an adaptive Neural Network controller with online backpropagation training for direct current regulation; and (4) detailed mathematical modeling of the PMSG power converter under various disturbances including wind speed variation and generator inertia changes.

The paper is organized as follows: Section 2 describes the wind turbine mode regions, and computes the gearbox ratio and blade length to determine the rated wind turbine speed. Section 3 elaborates the proposed pitch control system based on the Differential Evolution optimization method. Section 4 presents the dynamic equations of the Permanent Magnet Synchronous Generator. Section 5 explains the full-scale power converter control scheme and analyzes the two methods for stator quadrature-axis current control. Section 6 discusses the digital simulation results, and Section 7 draws the conclusions.

DESCRIPTION OF WIND TURBINE

A. Operation Region in PMSG Wind Turbine

As shown in Fig. 1(a), the PMSG turbine operates between cut-in speed (4 m/s) and cut-out speed (24 m/s), defined by three points: V_{cut-in}, minimum speed generating power; rated speed, where output is maximum; and $V_{cut-out}$, where the turbine stops.

B. Aerodynamics in PMSG Wind Turbine

The following nonlinear equations can be used to model the energy conversion of the PMSG wind turbine:

$$P_m = 0.5\rho A V_w^3 C_p \tag{1}$$

Where ρ is the density of air (kg/m^3), $A = \pi R^2$ is the area encompassing the turbine blades (m^2), R signifies the rotor radius (m), V_w denotes the wind speed (m/s), C_p indicates the power coefficient, and P_m represents the mechanical input power (Watt). For a given wind speed, the wind turbine's power depends on C_p. The wind turbine output characteristics are described by the relationship between C_p and λ and β, as shown in (2), [19]:

$$C_p(\lambda, \beta) = 0.73\left(151\lambda_i - 0.58\beta - 0.002\beta^{2.14} - 13.2\right)\ldots \\ \ldots \cdot e^{-18.4\lambda_i} \tag{2}$$

The expressions for λ, λ_i can be found in (3) and (4), respectively, where λ signifies the linear speed of the tip of the blade relative to the wind speed and β denotes the pitch angle.

$$\lambda = \frac{\omega_t R}{V_w} \tag{3}$$

$$\lambda_i = \frac{1}{\lambda + 0.02\beta} - \frac{0.003}{\beta^3 + 1} \tag{4}$$

Rotor turbine speed (rad/s) is ω_t. Fig. 1(b) shows C_p versus λ using (2) at various pitch angle β values. As β increases, maximum C_p decreases; at $\beta = 0$, optimal TSR yields maximum C_p (MPPT mode). For β exceeding zero, pitch control activates between rated and cut-out speed. Above rated wind speed, the generator and converter risk overload, so extracted power is restricted by reducing C_p. Turbine speed is held at $\omega_{t,rated}$ as wind speed varies, with λ calculated using (5).

$$\lambda = \frac{\omega_{t,rated}\, R}{V_w} \tag{5}$$

Using (6), the C_p equivalent to rated power is computed.

$$C_p = \frac{P_{rated}}{0.5 A \rho V_w^3} \tag{6}$$

Based on (4), (5), and (6)—all of which will be covered in more detail in the upcoming sections, the pitch angle value is found by applying the DE algorithm to solve the nonlinear equation (2).

$$R_{GB} = \frac{generator\ rated\ speed\ in\ r.p.m.}{turbine\ rated\ speed\ in\ r.p.m.} \tag{7}$$

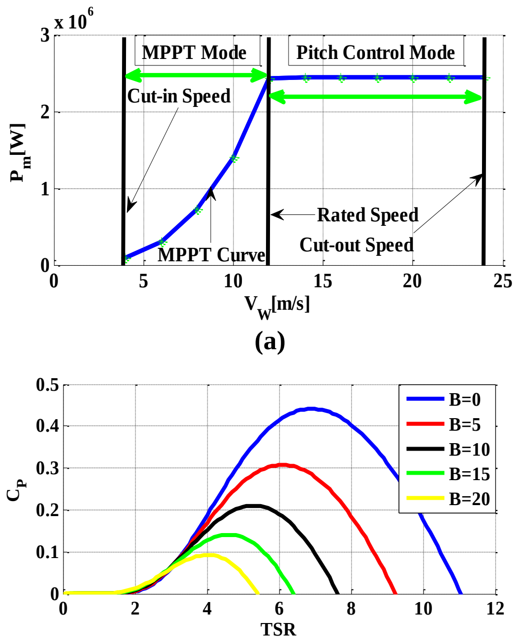

(a)

(b)

Fig. 1. PMSG characteristics: (a) Power speed curve; and (b) C_p plotted across β values.

The PMSG wind turbine's blade length is determined from generator data and the mechanical power equation, since accurate TSR requires correct blade length. First, λ_{opt} and $C_{p,max}$ are obtained — 6.9078 and 0.4412, respectively. Then, using $C_{p,max}$ at $V_w = 12\,m/s$ and the generator's rated value of 2.45 MW, blade length R=40.8555 m is found.

The gearbox raises the turbine rotor's low speed to one suitable for the generator. To compute gearbox ratio R_{GB}: first find rated turbine speed $\omega_{t,rated}$ by applying (5) with $V_w = 12\,m/s$ and $\lambda = \lambda_{opt}$, yielding $\omega_{t,rated}$ =2.0289 rad/s. Then, using (7) at the rated generator speed of 400 rpm and $n_{t,rated} = 19.3746\,\text{rpm}$, R_{GB} is computed as 20.6456. The following sections explain the pitch control process and the DE technique used to construct the pitch controller circuit and determine the necessary pitch angle for the variable-speed PMSG wind turbine.

PITCH CONTROL METHOD USING DE

The pitch angle is obtained by solving (2) using DE based on rated power and rated turbine speed in pitch control mode in the region from rated wind speed to cut-out speed according to Fig. 1(a) and Fig. 1(b) which will be explained below. Fig. 2 depicts that the pitch angle is obtained by a curve of V_w and β where the wind speed is the input and the output is the pitch angle. The section below will explain the DE algorithm.

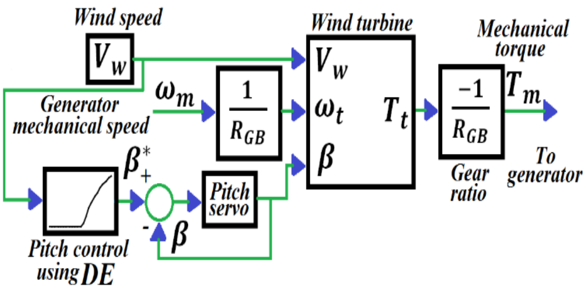

Fig. 2. Pitch control using the DE controller.

A. *Principles of DE*

Similar to other evolutionary algorithms on the overall structure, the DE algorithm is an evolutionary algorithm based on real coding. Three fundamental processes make up this system: crossover, mutation, and selection. The main steps of the standard DE algorithm are as follows, [20]:

- The initial population formation M individuals are generated randomly in the dimensions n space, as described in (8):

$$x_{ij}(0) = rand_{ij}(0,1)\left(x_{ij}{}^{U} - x_{ij}{}^{L}\right) + x_{ij}{}^{L} \qquad (8)$$

Where the jth chromosome's upper and lower boundaries are represented by $x_{ij}{}^{U}$ and $x_{ij}{}^{L}$, and $rand_{ij}(0,1)$ is a real number in the interval $[0,1]$.

- Mutation operator: Using a random selection of three individuals x_{p1}, x_{p2}, and x_{p3} from the population, allow $i \neq p_1 \neq p_2 \neq p_3$. Then, use the fundamental mutation operator as follows:

$$h_{ij}(t+1) = x_{p1j}(t) + F\left(x_{p2j}(t) - x_{p3j}(t)\right) \quad (9)$$

It is possible to write the mutation operator as in (10) if there is no local optimization problem.

$$h_{ij}(t+1) = x_{bj}(t) + F\left(x_{p2j}(t) - x_{p3j}(t)\right) \quad (10)$$

When F is a scaling factor, the difference operation is the key to the DE algorithm, and the difference vector is $x_{p2j}(t) - x_{p3j}(t)$.

The number of individuals in a population is indicated by the random integers p_1, p_2, and p_3, and the best individual in the current generation is indicated by $x_{bj}(t)$.

Utilization of Fig. 3 of the best individual data available in the current population allows for an acceleration of the convergence rate.

- The purpose of the cross operator is to broaden the group's variety. The operator is as follows:

$$v_{ij}(t+1) = \begin{cases} h_{ij}(t+1), rand\,l_{ij} \le CR \\ x_{ij}(t), rand\,l_{ij} > CR \end{cases} \quad (11)$$

Given a random number, rand l_{ij}, and a crossover probability, CR, such that $CR \in [0,1]$.

- Selection operator to ascertain if $x_i(t)$ belongs to the subsequent generation, the evaluation functions are compared using vectors $v_{ij}(t+1)$ and $x_{ij}(t)$, as shown in (12):

$$x_i(t+1) = \begin{cases} v_i(t+1), f\left(v_{i1}(t+1),\ldots,v_{in}(t+1)\right)\ldots. \\ < f\left(x_{i1}(t),\ldots,x_{in}(t)\right) \\ x_{ij}(t), f\left(v_{i1}(t+1),\ldots,v_{in}(t+1)\right)\ldots \\ \geq f\left(x_{i1}(t),\ldots,x_{in}(t)\right) \end{cases} \quad (12)$$

Steps (2) through (4) should be repeated until the maximum evolutionary iteration G is attained, where $j = 1,2,\ldots,n$. Fig. 3 shows how DE works in general.

B. DE Controller for Pitch Control Mode

To limit output power and protect the wind turbine from high wind speeds between rated and cut-out speed, the DE controller obtains the necessary pitch angle for each wind speed above the rated value. Key requirements: the rated power $P_{m,rated}$ =2.45 MW ($V_w = 12-24\,m/s$); rated turbine speed $\omega_{t,rated}$ =2.0289 rad/s ($V_w = 12-24\,m/s$). Defining the object function requires a one-variable equation, with the constraint $0 \leq \beta \leq 30$, where $\beta_{min} = 0$ and $\beta_{max} = 30$. Table 1 lists the DE parameter settings used here.

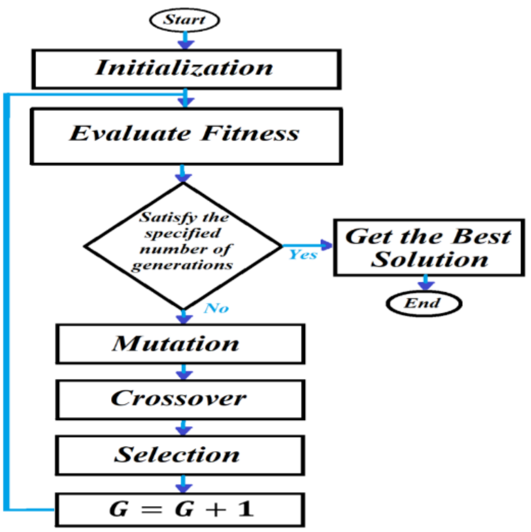

Fig. 3. Flowchart of DE technique.

Table 1

Parameters of DE

DE parameter setting	Value
Mutation factor ***F***	0.4
Crossover factor ***CR***	0.7
Group size	35
No. of iterations ***G***	150

The object function F used here is given as in (13):

$$F = 0.73\left(151\lambda_i - 0.58\beta - 0.002\beta^{2.14} - 13.2\right)\ldots \\ \ldots e^{-18.4\lambda_i} - C_p = 0, \quad (13)$$

where $\lambda_i = \dfrac{1}{\lambda + 0.02\beta} - \dfrac{0.003}{\beta^3 + 1}$ at $\lambda = \dfrac{\omega_{t,rated}\, R}{V_w}$, $C_p = \dfrac{P_{m,rated}}{0.5A\rho V_w{}^3}$. Under specified parameters, DE resolves the equation; pitch angle at $V_w = 13\,m/s$ fluctuates (Fig. 4), converging after iterations (Fig. 5). Fig. 6 relates angle to wind speed, activating once wind exceeds rated value. Fig. 7(a)-(b) show C_p, TSR decreasing with angle, modeled via lookup table.

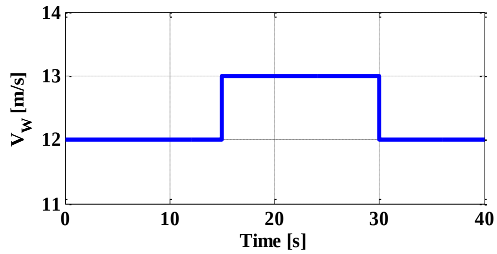

Fig. 4. Wind speed variation.

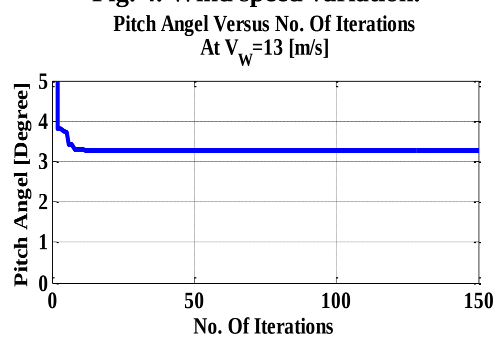

Fig. 5. Pitch angle β versus iterations number.

The equation for Fig. 8 is produced using the curve fitting property in the MATLAB program, as described in (14). Fig. 9 shows the whole model of the pitch control system utilizing DE.

$$\beta(V_w) = p_1 V_w{}^9 + p_2 V_w{}^8 + p_3 V_w{}^7 + p_4 V_w{}^6 + \ldots \\ \ldots p_5 V_w{}^5 + p_6 V_w{}^4 + p_7 V_w{}^3 + p_8 V_w{}^2 + p_9 V_w{}^1 + p_{10} \quad (14)$$

Where $p_1, p_2, \ldots, and\ p_{10}$ are the coefficients and the range of V_w is $12 < V_w \leq 24$.

Table 2 displays the wind turbine parameters used in this paper. The DE optimization method plays a crucial role in accurately estimating the correct pitch angle values for wind speeds that exceed the rated value in PMSG wind turbines. Proper estimation of these pitch angles is essential, as it significantly impacts the mechanical power output. If the pitch angles are not accurately determined, it can lead to excessive stress on the power converter components, potentially causing damage.

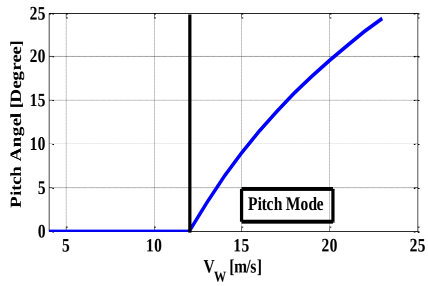

Fig. 6. Pitch angle β in a variable speed mode.

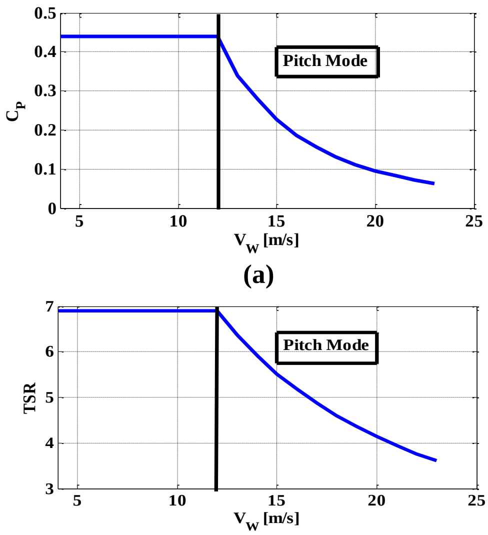

(a)

(b)

Fig. 7. Pitch control mode: (a) The power coefficient C_p ; (b) TSR λ .

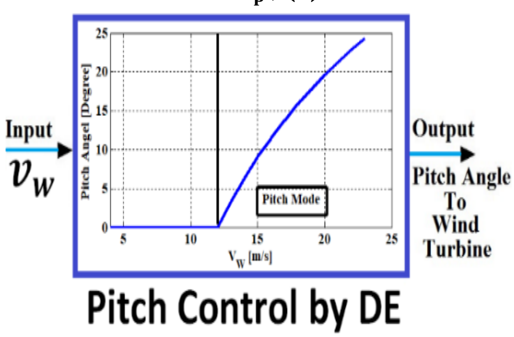

Fig. 8. Pitch angle β versus wind speed V_w .

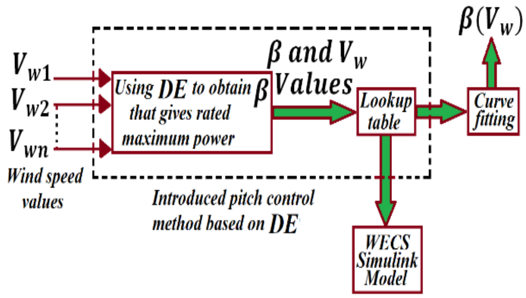

Fig. 9. Pitch control using DE.

Table 2

Characteristics of wind turbines

Parameter	Symbol	Value
Air density	P	1.225 Kg/ m^3
Number of blades	N_{blades}	3
Rated wind speed	$V_{\text{Rated-wind\_}}$	12 m/s
Cut-in/out wind speed	$V_{cut-in}/V_{cut-out}$	4/25 m/s
Max C_p (MPPT)	C_{pmax}	0.4412
Optimal λ (MPPT)	λ_{opt}	6.9078
Rated maximum power	P_{rated}	2.45 MW
Maximum/minimum pitch angle	$\beta_{Max/Min}$	30/0 degree

PMSG MODEL

Fig. 10 illustrates the PMSG-based WECS. The dynamic model, as described in equations (15)–(20), depicts the behavior of a 2.45 MW PMSG utilizing the d-q axis synchronous reference frame [21]. Table 3 contains the parameters of the PMSG.

$$v_{qs} = -R_s i_{qs} + \omega_r \lambda_{ds} + \frac{d}{dt}\lambda_{qs} \tag{15}$$

$$v_{ds} = -R_s i_{ds} - \omega_r \lambda_{qs} + \frac{d}{dt}\lambda_{ds} \tag{16}$$

$$\lambda_{ds} = -L_d i_{ds} + \lambda_r \tag{17}$$

$$\lambda_{qs} = -L_q i_{qs} \tag{18}$$

$$v_{qs} = -R_s i_{qs} + \omega_r \left(-L_d i_{ds} + \lambda_r\right) - L_q \frac{d}{dt} i_{qs} \tag{19}$$

$$v_{ds} = -R_s i_{ds} + \omega_r L_q i_{qs} - L_d \frac{d}{dt} i_{ds} \tag{20}$$

The stator resistance is denoted by R_s. In addition, the q and d-axis stator voltages are denoted as v_{qs} and v_{ds}, respectively. i_{qs} and i_{ds} represent the stator currents along the q and d axes, respectively.

The connections of the q- and d-axis stator fluxes are denoted by λ_{qs} and λ_{ds}, respectively.

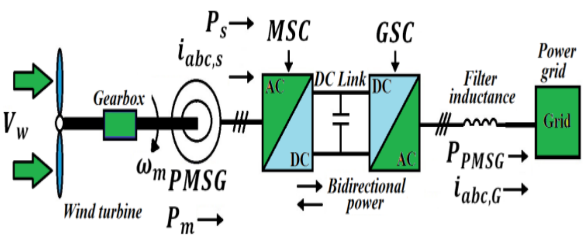

Fig. 10. PMSG based WECS.

In a PMSG wind turbine, the rotor flux is constant and is denoted by λ_r. Moreover, the stator q and d-axis self-inductances are denoted by L_q and L_d, respectively. The rotor's electrical angular speed is represented by ω_r. The stator side's active and reactive power outputs are explained as follows in (21) – (22):

$$P_s = \frac{3}{2}\left(v_{qs}i_{qs} + v_{ds}i_{ds}\right) \tag{21}$$

$$Q_s = \frac{3}{2}\left(v_{qs}i_{ds} - v_{ds}i_{qs}\right) \tag{22}$$

Table 3

PMSG parameters

Parameter	Value
$\boldsymbol{P_{m,rated}}$	2.45 MW
Rated line-line voltage	4000 V (rms)
Rated stator frequency	53.33 Hz
Rated rotor speed	400 rpm
P	8
$\boldsymbol{T_{m,rated}}$	58.4585 kN-m
$\boldsymbol{J}$	1558.9 $Kg.m^2$
$\boldsymbol{R_s}$	24.21 $m\Omega$
$\boldsymbol{L_d}$	9.816 mH
$\boldsymbol{L_q}$	9.816 mH
Rated rotor flux linkage	4.971 Wb (rms)
DC link voltage, $\boldsymbol{V_{dc}}$	7000 V
DC link capacitor, $\boldsymbol{C}$	90 mF
Grid frequency	60 Hz

The following describes the total active and reactive powers that PMSG produces (23) – (24):

$$P_{PMSG} = P_{total} = P_s \tag{23}$$

$$Q_{total} = Q_s \tag{24}$$

When P_{total} is negative, and PMSG is supplying the grid with power. The machine generates an electromagnetic torque T_e, which is expressed as follows in terms of flux linkages and current (25):

$$T_e = \frac{3P}{2}\left(\lambda_r i_{qs} - \left(L_d - L_q\right) i_{ds} i_{qs}\right) \tag{25}$$

CONTROL OF PMSG WECS

The power converter, comprising the Grid Side Converter (GSC) and MSC, achieves PMSG control. Two techniques regulate MSC current for rated power control: PI controller with optimal β via DE, and NN controller.

A. Design of MSC Controller

The power converter links PMSG stator to grid via ZDPC control, a standard vector-control FOC strategy, setting i_{ds} to zero so stator current equals i_{qs}. MSC holds rotor speed at rated value via i_{qs}; the regulator maintains this in pitch control, ignoring friction as in (26). The generator's inertia is denoted by J. The mechanical torque T_m can be expressed as follows in the case where the wind speed V_w exceeds the rated wind speed:

$$\frac{d}{dt}\omega_r = \frac{P}{J}\left(T_m - T_e\right) \tag{26}$$

$$T_m = \frac{P_{m,rated}}{\omega_{t,\text{ rated}}} \tag{27}$$

Where $P_{m,rated}$ is the rated power of PMSG wind turbine, (26) can be rewritten as follows:

$$\frac{J}{P}\frac{d}{dt}\omega_r = \left(T_m - T_e\right) = \delta_{\omega r} = K_{\omega r}\left(\omega_r^* - \omega_r\right) \tag{28}$$

Where ω_r^* represents the constant reference rated rotor electrical angular speed. Also, $\delta_{\omega r}$ and $K_{\omega r}$ are the output of the PI speed controller, and the transfer function of the speed regulator is described as $K_{\omega r}=\left(K_{P\omega r}+\frac{K_{I\omega r}}{s}\right)$, respectively. After that, (28) will be:

$$\frac{J}{P}s\omega_r=\left(T_m-T_e\right)=\left(K_{P\omega r}+\frac{K_{I\omega r}}{s}\right)\omega_r^{*}-\ldots \quad (29)$$
$$\ldots\left(K_{P\omega r}+\frac{K_{I\omega r}}{s}\right)\omega_r$$

Where $s=\frac{d}{dt}$ signifies Laplace operator. After that, the transfer function must be obtained as follows:

$$\frac{\omega_r}{\omega_r^{*}}=\frac{\frac{P}{J}\left(sK_{P\omega r}+K_{I\omega r}\right)}{s^2+s\frac{PK_{P\omega r}}{J}+\frac{PK_{I\omega r}}{J}} \quad (30)$$

The stability of the system is upheld by optimizing the locations of the closed-loop eigenvalues through the selection of the PI controller's gains.

Equation (31) outlines a transfer function denominator of the second order.

$$s^2+\sqrt{2}\,\omega_0 s+\omega_0^2=0 \quad (31)$$

Where the circle radius is ω_0, and the switching frequency is $\omega_{sw}=6283.2\,rad/s$, $\omega_{outer}=\frac{\omega_{sw}}{0.9}$. Comparing (31) parameters with the denominator of the transfer function derived in (30) helps determine the PI controller gains.

The resulting outer-loop rotor speed controller parameters for the MSC design $\omega_{0\omega r}=\frac{\omega_{outer}}{1000}\,rad/s$ are detailed in Table 4.

Table 4

Speed regulator parameters

Speed regulator gains	Values
$\mathbf{K}_{\mathbf{P}\omega\mathbf{r}}=\sqrt{2}\,\omega_{0\omega r}\frac{\boldsymbol{J}}{\boldsymbol{P}}$	1923.9
$\mathbf{K}_{\mathbf{I}\omega\mathbf{r}}=\frac{\boldsymbol{J}}{\boldsymbol{P}}\omega_{0\omega r}^{2}$	9497.2

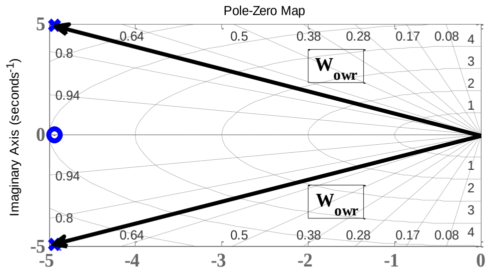

Fig. 11. Poles location for the speed regulator.

In Fig. 11, it's evident that the speed regulator poles for the derived transfer function reside on the left side of the s-plane. The electromagnetic torque function, expressed in terms of i_{qs}, is derived by substituting $i_{qs}=i_s$ and $i_{ds}=0$ into equation (25).

$$\begin{cases} T_e=\frac{3P}{2}\left(\lambda_r i_{qs}\right) \\ \left(T_m-T_e\right)=\delta_{\omega r}\end{cases} \quad (32)$$

A further substitution of (32) into (28) gives:

$$i_{qs}=i_{qs}^{*}=\frac{2}{3P\lambda_r}\left(T_m-\delta_{\omega r}\right) \quad (33)$$

So, (19) can be written as:

$$v_{qs}=-R_s i_{qs}-L_q\frac{d}{dt}i_{qs}+-\omega_r L_d i_{ds}+\omega_r\lambda_r \quad (34)$$

$$v_{qs}=-\delta_{qs}+-\omega_r L_d i_{ds}+\omega_r\lambda_r \quad (35)$$

Where δ_{qs} denotes the output of the current regulator in the q-axis.

$$\delta_{qs}=R_s i_{qs}+L_q\frac{d}{dt}i_{qs}=\left(K_{Pqs}+\frac{K_{Iqs}}{s}\right)\left(i_{qs}^{*}-i_{qs}\right) \quad (36)$$

By taking Laplace transformer. So, (36) can be written as follows:

$$R_s i_{qs}+L_q s i_{qs}=\left(K_{Pqs}+\frac{K_{Iqs}}{s}\right)i_{qs}^{*}-\left(K_{Pqs}+\frac{K_{Iqs}}{s}\right)i_{qs} \quad (37)$$

After that, as indicated below, the transfer function for the current regulator in the q-axis must be obtained as follows:

$$\frac{i_{qs}}{i_{qs}{}^{*}}=\frac{\frac{1}{L_q}\left(sK_{Pqs}+K_{Iqs}\right)}{s^2+s\frac{1}{L_q}\left(R_s+K_{Pqs}\right)+\frac{1}{L_q}K_{Iqs}} \quad (38)$$

Upon comparing the parameters in (31) with those in the denominator of the transfer function obtained through derivation in equation (38), the PI parameters for the current controller are established. Subsequently, the PI parameters for the stator current regulator in the d and q-axes for the inner loop of the MSC design are determined as $\omega_0=\omega_{outer}$.

In Fig. 12, it's evident that the current regulator poles for the derived transfer function reside on the left side of the s-plane.

Table 5

Parameters of stator current regulator

Stator current regulator gains	Values
$\boldsymbol{K_{Pqs}=K_{Pds}=\sqrt{2}\,\omega_0\,L_q-R_s}$	96.8899
$\boldsymbol{K_{Iqs}=K_{Ids}=L_q\,\omega_0{}^2}$	$4.784*10^5$

To maintain the reference direct current axis equation at zero in the MSC control scheme, the current regulator is applied, in accordance with the (ZDPC) principle.

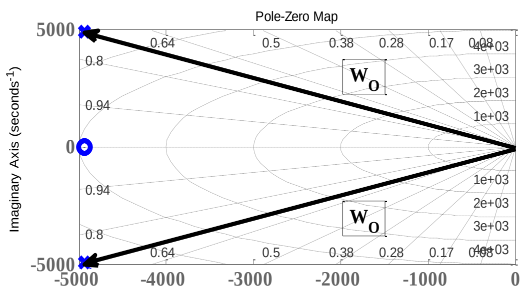

Fig. 12. Poles location for stator current regulator.

Consequently, (20) can be reorganized as follows:

$$v_{ds}=-R_s i_{ds}-L_d\frac{d}{dt}i_{ds}+\omega_r L_q i_{qs} \quad (39)$$

$$v_{ds}=-\delta_{ds}+\omega_r L_q i_{qs} \quad (40)$$

Where δ_{ds} is the output of the PI controller in the d-axis as follows:

$$\delta_{ds}=R_s i_{ds}+L_d\frac{d}{dt}i_{ds} \quad (41)$$

$$\delta_{ds}=\left(K_{Pds}+\frac{K_{Ids}}{s}\right)\left(i_{ds}{}^{*}-i_{ds}\right) \quad (42)$$

transformer, So, (41)-(42) can be written as follows:

$$R_s i_{ds}+L_d s i_{ds}=\left(K_{Pds}+\frac{K_{Ids}}{s}\right)i_{ds}{}^{*}-\left(K_{Pds}+\frac{K_{Ids}}{s}\right)i_{ds} \quad (43)$$

Following that, the transfer function for the current regulator in the q-axis must be derived in the following manner:

$$\frac{i_{ds}}{i_{ds}{}^{*}}=\frac{\frac{1}{L_d}\left(sK_{Pds}+K_{Ids}\right)}{s^2+s\frac{1}{L_d}\left(R_s+K_{Pds}\right)+\frac{1}{L_d}K_{Ids}} \quad (44)$$

Upon comparing the parameters in (31) with the denominator of the derived transfer function in equation (44), it is significant to determine the PI coefficients of the current controller. Subsequently, Table 5 demonstrates how the PI parameters for the stator current regulators in the d and q axes correlate. It should be noted that equations (35) and (40) are the two primary equations used in constructing MSC control circuits.

B. SVM for MSC

C.

Equations (35) and (40) calculate the MSC reference voltage signals $v_{qs}{}^{*}$ and $v_{ds}{}^{*}$, used as inputs to the Space Vector Modulation (SVM) block Fig. 13(a). Using the $(d-q)/(\alpha-\beta)$ transformation, these d-q-0 frame voltages convert to two-phase variables v_α and v_β within the stationary $(\alpha-\beta)$ frame, forming the reference vector $\overrightarrow{v_{ref}}$. Once the reference vector is determined, (46) and (47) compute the modulation index m_a and sector number, while (48) determines dwell durations. Fig. 13(b) generates the switching sequence and gate signals for the MSC's six switches, ensuring SVM-based output voltage matches the reference voltage precisely.

$$\begin{cases} \overrightarrow{v_{ref}} = v_{ref}\, e^{j\theta} \\ v_{ref} = \sqrt{{v_\alpha}^2 + {v_\beta}^2} \\ \theta = \tan^{-1} \dfrac{v_\beta}{v_\alpha} \end{cases} \tag{45}$$

$$m_a = \frac{\sqrt{3}\, v_{ref}}{V_{dc}} \tag{46}$$

$$\theta' = \theta - (k-1)\pi/3 \tag{47}$$

For the specified range $0 \le \theta' < \pi/3$, the parameter k=1, 2 ,…, 6 represents the designated sectors, respectively.

$$\begin{cases} T_a = T_s m_a \sin\left(\dfrac{\pi}{3} - \theta\right) \\ T_b = T_s m_a \sin(\theta) \\ T_o = T_s - T_a - T_b \end{cases} \tag{48}$$

D. Design of MSC based NN controller

Instead of using a PI controller with the reference rated rotor speed equation, this method employs an NN controller to directly regulate the stator MSC quadrature-axis current i_{qs}, maintaining rated output power. Its steady-state computation serves as the input value, achieving pitch control through direct current regulation.

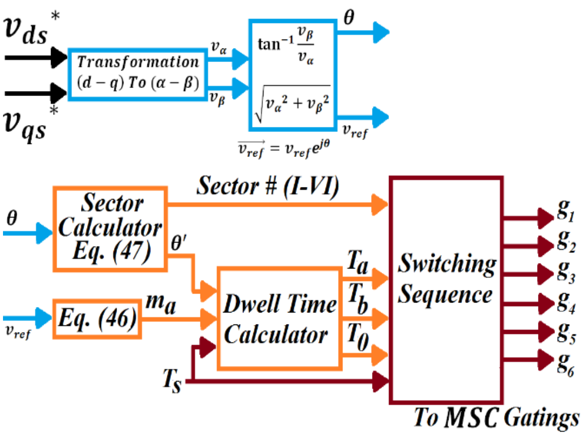

(a)

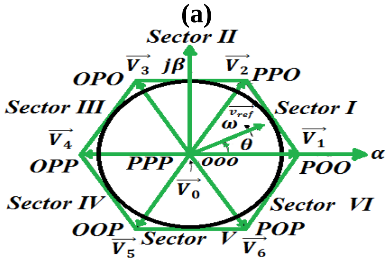

(b)

Fig. 13. SVM: (a) Structure, (b) Control diagram.

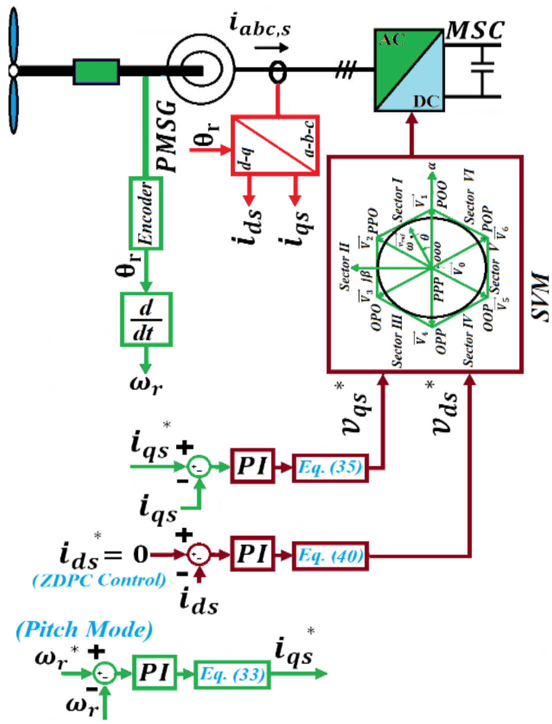

Fig. 14. MSC block diagram.

E. Fundamentals of NN Controller

In Fig. 15, the NN controller comprises input, hidden, and output layers; the hidden layer performs all computations. Its role is to estimate the MSC stator quadrature-axis current that regulates torque and limits output power during pitch control. Each hidden-layer neuron has weight w, bias b, and activation function f, using a sigmoid activation function (SAF), nine hidden-layer neurons, trained via the online delta-rule backpropagation algorithm.

Weights are adjusted in the reverse pass until the response matches the desired response, using backpropagation to fully train the NN.

The real MSC current i_{qs} is input x_1, while desired output d_j reflects the steady-state reference current needed for rated power operation. Comparing NN output with the required signal updates weights and biases, yielding reference current i_{qs}^*, at a learning rate of 0.5.

- Hidden layer forward propagation follows the single-neuron summation principle $(l=1)$.

$$s_j = \sum_{i=1}^{N} w_{ji} x_i + b_j \tag{49}$$

- Here, the terms represent the weighted sum s_j, bias b_j, and weight w_{ji} respectively; initial values are assumed for the hidden layer's biases and weights $(j = 1,2,3)$.

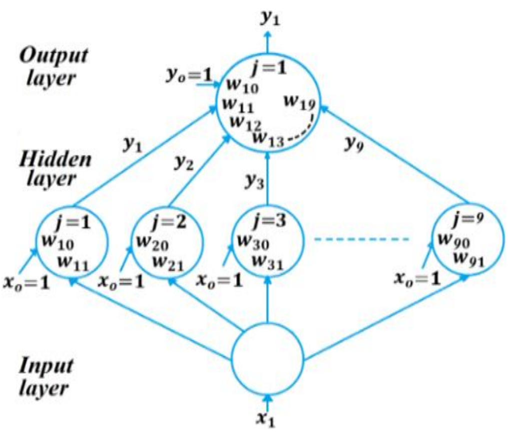

Fig. 15. NN with three-layer feedforward.

- Utilizing SAF in the hidden layer $(j = 1 to 9)$, neuron output y_j is calculated as in (50).

$$y_j = \frac{1}{1+e^{-s_j}} \tag{50}$$

- For the output layer $(l = 2)$, the single-neuron law is as follows (49).
- It is expected that the output layer's weight and bias initial values start at these values.
- According to the SAF in the output layer $(j = 1)$, the neuron output y_1 as in (50).
- The error e_p, computed as shown in (51) during backpropagation, represents the variance between the required signal and NN's output $(l = 2)$.

$$e_p = d_j - y_j \tag{51}$$

- Output layer error function δ_j assessed (52).

$$\delta_j = y_j\left(1 - y_j\right)e_p \tag{52}$$

- As shown in equation (53), the output layer's weights and biases are adjusted using the delta rule for backpropagation.

$$\Delta w_{ji}(kt) = \gamma \delta_j x_i \tag{53}$$

- Weight increment $\Delta w_{ji}(kt)$ is denoted; (54) lists updated output layer weights and biases.

$$w_{ji}(kt) = w_{ji}(k-1)t + \Delta w_{ji}(kt) \tag{54}$$

- Regarding the hidden layer $(l = 1)$, the values of $\left[\delta_j\right]_l$ would be as follows:

$$\left[\delta_j\right]_l = \left[y_j\left(1 - y_j\right)\right]_l \left[\sum_{j=1}^{N} w_{ji}\delta_j\right]_{l+1} \tag{55}$$

- As a result, weight increments for the hidden layer are determined using the delta rule per (54); this repeats until the objective function is minimal, updating weights and biases.

Unlike Levenberg-Marquardt, this update requires no Jacobian matrix construction or matrix inversion; each update uses only the instantaneous error and input at the current sample via simple multiply-accumulate operations and a fixed learning rate 0.5, making it feasible at the model's 5 µs discrete sample time.

F. Design of the MSC Current Controller During Pitch Control Mode

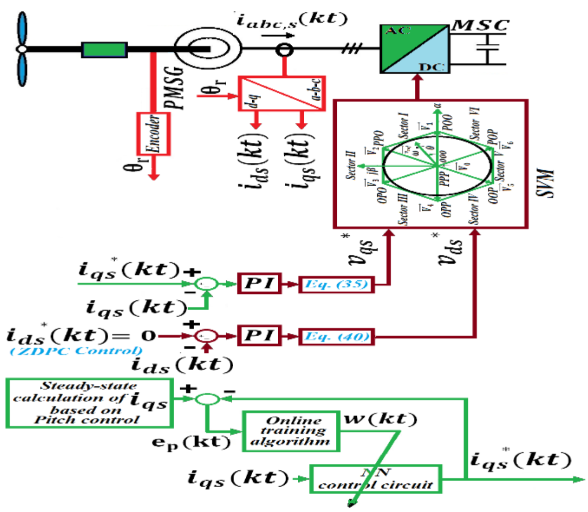

Fig. 16. MSC block diagram controlled by NN.

As shown in Fig. 16, once in pitch control mode, the NN controller regulates MSC stator current to maintain rated power with ZDPC maintaining $i_{ds} = 0$, $i_{qs} = i_s$. The discrepancy between steady-state MSC current and reference current $i_{qs}^{*}(kt)$ forms error signal $e_p(kt)$, driving backpropagation to adjust weights, converging $i_{qs}^{*}(kt)$ toward the desired value. Per Fig. 17, steady-state i_{qs} is given by (56), where ω_m, T_m, $\omega_{m,pu}$ are mechanical speed, torque, and per-unit speed.

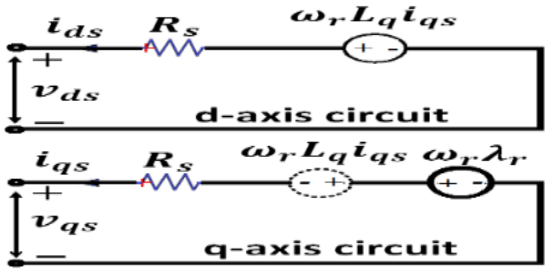

Fig. 17. The generator's steady-state model.

$$\begin{cases} \omega_t = \omega_{t,\,rated} = \dfrac{\lambda V_w}{R} \\ \omega_{m,\,rated} = R_{GB}\omega_{t,\,rated} \\ \omega_{m,pu} = \dfrac{\omega_{m,rated}}{\omega_{m,\,rated}} \\ T_m = T_e = T_{m,\,rated}\left(\omega_{m,pu}\right)^2 \\ i_{ds} = 0 \text{ for ZDPC control} \\ i_{qs} = \dfrac{T_e}{1.5P\lambda_r} \end{cases} \tag{56}$$

Finally, as shown in Fig. 16, the reference MSC d and q-axis currents, i_{ds}^{*} and i_{qs}^{*}, respectively, are derived. Also, in the same inner control loop as in the previous case, both the direct i_{ds}^{*} and quadrature i_{qs}^{*} axis reference currents are used to obtain the reference voltage control signals of the MSC circuit v_{ds}^{*} and v_{qs}^{*}, which are used as the input signals to the SVM block diagram to obtain the necessary switch control signals for MSC.

G. Design of GSC Controller

The GSC control strategy targets unity power factor while regulating DC-link voltage, using the Stator Voltage Orientation Control (SVOC) method. Grid quadrature-axis voltage v_{qg} is set to zero, while direct-axis voltage $v_{dg} = v_g$. Following the standard power-balance and PI design approach, the DC-link voltage transfer function and PI gains $K_{P,dc}$ and $K_{I,dc}$ are derived as:

$$C\frac{dV_{dc}}{dt} = \delta_{dc} = K_{dc}\left(V_{dc}^{*} - V_{dc}\right) \tag{57}$$

$$\frac{V_{dc}}{V_{dc}^{*}} = \frac{\frac{1}{C}\left(sK_{P,dc} + K_{I,dc}\right)}{s^2 + s\frac{1}{C}K_{P,dc} + \frac{1}{C}K_{I,dc}} \tag{58}$$

Table 6 summarizes the resulting DC voltage regulator gains with $\omega_{0dc} = \dfrac{\omega_{sw}}{100}$:

Table 6

The DC voltage regulator's parameters

DC voltage regulator gains	Values
$\boldsymbol{K_{P,dc} = \sqrt{2}\,\omega_{0dc}\,C}$	79.9719
$\boldsymbol{K_{I,dc} = C\,\omega_{0dc}^{2}}$	$3.5531 \cdot 10^3$

Similarly, applying the same PI-tuning method to the GSC inner current loop yields the current regulator transfer function:

$$\frac{i_{d,GSC}}{i_{d,GSC}^{*}} = \frac{\frac{1}{L_F}\left(s\,K_{pdg} + K_{idg}\right)}{s^2 + s\frac{1}{L_F}\left(R_F + K_{pdg}\right) + \frac{1}{L_F}K_{idg}} \tag{59}$$

Where R_F and L_F denote the resistance and inductance of the R-L filter, respectively. Table 7 gives the resulting GSC current regulator gains with $\omega_{0c} = \dfrac{\omega_{sw}}{10}$:

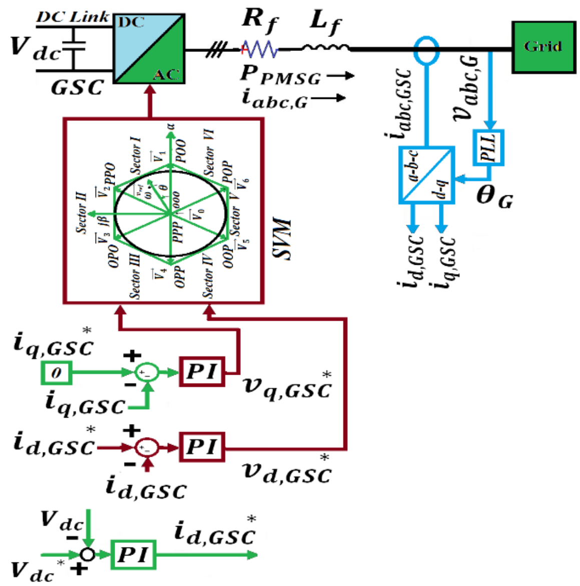

Fig. 18. GSC block diagram.

Table 7

GSC current regulator parameters

GSC current regulator gains	Values
$K_{pdg} = K_{pqg} = \sqrt{2}\,\omega_{0c}\,L_F - R_F$	0.8876
$K_{idg} = K_{iqg} = L_F\,\omega_{0c}^{\,2}$	394.7842

Fig. 18 shows the complete GSC control block diagram, combining the outer DC-voltage loop with the inner d-q current loops, using SVM-based switching signals.

RESULTS AND DISCUSSION

For the two aforementioned pitch control system methods, Matlab/Simulink is used to implement the 2.45 MW PMSG control structure. Several conditions are used to run the simulation, including the following: changes in wind speed and modifying the inertia of the generator.

A. Case 1: Variation in Wind Speed

To validate the effectiveness of the pitch control system mentioned above during wind speed fluctuations, a simulation is performed for a 2.45 MW PMSG-based WECS. Table 3 outlines the PMSG parameters, while Fig. 19 illustrates the variations in wind speed.

The wind turbine switches to pitch control mode when the wind speed surpasses the rated wind speed ($V_w = 12\,m/s$) and when $C_p < 0.44$, $\lambda < 6.9$ at $\beta > 0$. Fig. 20 and 21 depict the time responses of C_p and λ for different wind speeds, respectively. Fig. 20 and 21 show that C_p and TSR under pitch control meet the predicted DE values (Fig. 7) above the rated wind speed; the NN controller responds rapidly, reaching steady-state promptly, while the speed regulator's TSR exhibits overshoot, potentially affecting all PMSG parameters—demonstrating the NN controller's superior MSC current regulation.

In pitch control mode, generator torque and speed remain constant at rated values (Fig. 22 and 23); Fig. 24 shows the MSC stator quadrature-axis current response, i_{qs}.

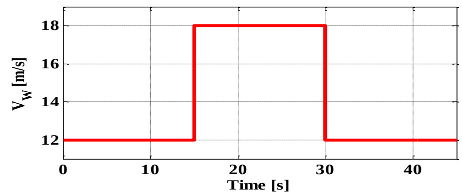

Fig. 19. The wind speed in Matlab/Simulink.

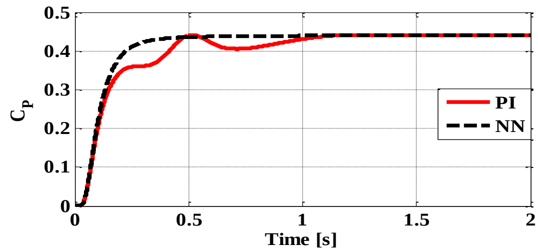

Fig. 20. Response of power coefficient C_p.

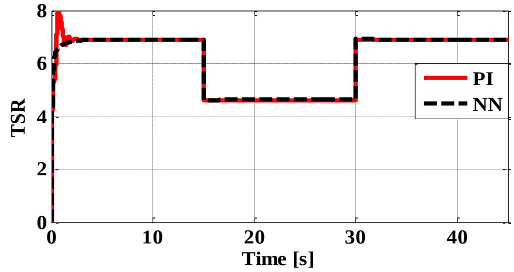

Fig. 21. Response of TSR for PMSG.

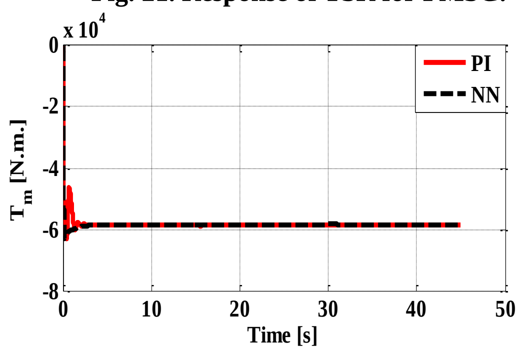

Fig. 22. Response of generator mechanical torque

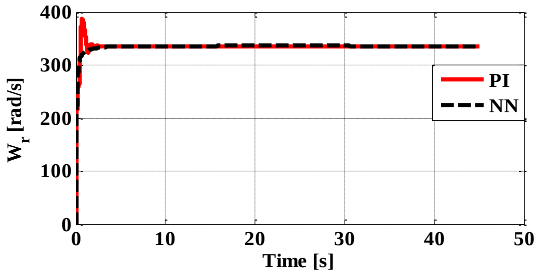

Fig. 23. Response of generator electrical speed.

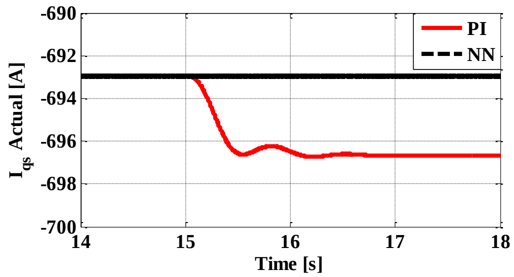

Fig. 24. Response of the MSC i_{qs}.

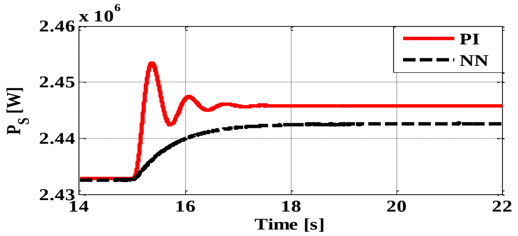

Fig. 25. Response of stator active power of PMSG.

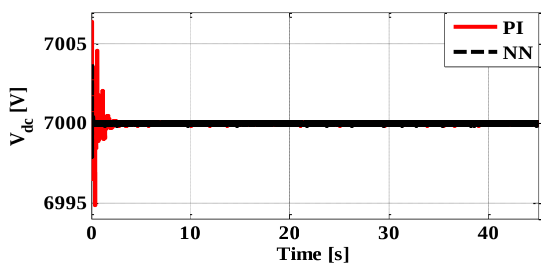

Fig. 26. Response of DC-link voltage.

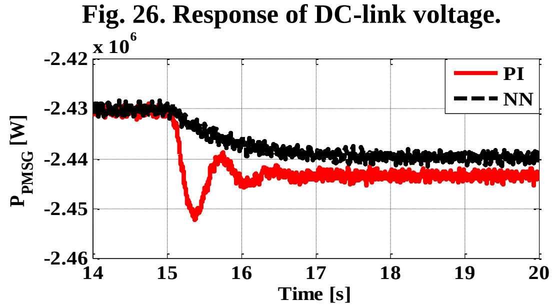

Fig. 27. Response of PMSG active power.

Notably, there's a significant overshoot in current i_{qs} when a speed regulator is used compared to an NN controller, potentially impacting the functioning and lifespan of the MSC circuit components. Additionally, Fig. 25 displays the response of the stator's active power.

Fig. 26 illustrates the continuous preservation of a stable DC-link voltage throughout the operational process. Finally, the estimated maximum power of the wind speed is given in Fig. 27, which represents the overall response of the active power output of the PMSG.

Table 8

Rated output power in ideal and practical cases

Case	$P_{PMSG}\,(W)$	$P_{loss}\,(W)$
Ideal case	2.43 MW	0
Practical case (PI)	2.444 MW	14 kW
Practical Case (NN)	2.437 MW	7 kW

Table 9

Finding Steady-State Error (SSE) percentage

Parameter	SS	PI	NN	SSE % (PI)	SSE % (NN)
i_{qs} (A)	692.959	696.67	692.957	-0.5355	0.00028
P_s (MW)	2.4311	2.44576	2.44256	-0.603	-0.471

Table 10

Finding max overshoot M_P at J=1558.9 $Kg.m^2$

Parameter	PI	NN
M_P % in TSR	17.39%	0%
M_P % in T_m	20.46%	0%
M_P % in P_{PMSG}	72.9%	0%
M_P % in ω_r	15.39%	0%
M_P % in V_{dc}	0.085%	0%

The key advantages of using NN controller in regulating the stator MSC quadrature-axis current compared to the PI controller in wind turbine pitch control systems can be represented into two main points, the first because the stator MSC quadrature-axis current is sensitive to any variation in wind speed under using PI controller as illustrated in Fig. 24 despite of evaluation its gain parameters well and the second is as a result of increasing the stator MSC quadrature-axis current, the stator active power and the active output power will increase and cause an excessive stress on the generator and the power converter components as depicted in Fig. 25, Fig. 27, and Table 8, respectively. Here, a solution to this problem is offered by controlling the stator MSC quadrature-axis current via NN controller which controls the current at its steady-state value as it is the input to the desired value terminal of NN as illustrated in Fig. 24 and Table 9. This minimizes power increase above rated value during wind speed variation (Fig. 25), reducing generator/converter stress and extending component lifespan. Controlling stator MSC current via the NN controller optimizes power generation to its minimum increase (Table 9). Both controllers maintain rated output, but NN outperforms PI: the speed regulator overshoots; NN mitigates current overshoot risk (Table 10); current stabilizes quickly.

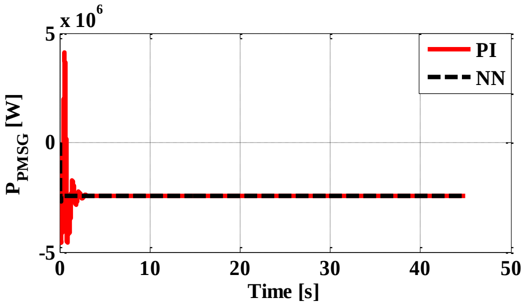

Fig. 28. PMSG active power under $J = 28\,\mathrm{Kg.m^2}$.

B. Case 2: Changing of Generator Inertia

To examine how generator inertia affects the pitch control scenarios, the system was simulated using the previously mentioned wind speed. Fig. 28 shows the resulting PMSG output power response under a specified generator inertia. Both NN and PI controllers regulate output power to rated levels, though stabilization takes time. Across varying wind speeds and inertia conditions, PMSG parameters exhibit similar overshoot and excess power, confirming the NN controller's superior performance over the PI-based system.

CONCLUSION

This paper compares two pitch control strategies for PMSG wind turbines, both aimed at regulating the stator MSC quadrature-axis current to enable swift pitch control and prevent high current overshoots that can damage MSC components and trigger alarms. The first method uses PI-based speed regulator, tuned via second-order system, to hold rotor electrical angular speed at its rated value through pitch angles obtained via Differential Evolution. The second employs an adaptive NN controller, trained online with online delta-rule backpropagation algorithm, to directly regulate stator MSC quadrature-axis current against its steady-state reference. Both achieve rated power once wind speed exceeds the rated limit, but simulation results show NN controller reaches steady state faster and, unlike PI controller, virtually eliminates current overshoot, extending MSC component lifespan and lowering operational costs.

REFERENCES

[1] Elngar, A.E., Sabik, A.S., Adel, A.H., Nada, A.S. Comparative performance evaluation of wind energy systems using doubly fed induction generator and permanent magnet synchronous generator. *Wind*, 2025, vol. 5, no. 4, p. 31.

[2] Jung, S.-Y., Kang, D., Palanimuthu, K., Joo, Y.H. Design of 20 MW direct-drive permanent magnet synchronous generators for wind turbines based on constrained many-objective optimization. *Wind Energy*, 2024, vol. 27, no. 9, pp. 847–872.

[3] Desalegn, B., Gebeyehu, D., Tamirat, B. Wind energy conversion technologies and engineering approaches to enhancing wind power generation: A review. *Heliyon*, 2022, vol. 8, no. 11, p. e11263.

[4] Nguyen, T.-T., Vu, T., Ortmeyer, T., Stefopoulos, G., Pedrick, G., MacDowell, J. Real-time transient simulation and studies of offshore wind turbines. *IEEE Transactions on Sustainable Energy*, 2023, vol. 14, p. 1474.

[5] Venkateswaran, R., Lee, S.R., Joo, Y.H. Stability augmentation of pitch angle control for maximum power extraction of PMSG-based WTS with pitch actuator uncertainty via L1 adaptive scheme. *International Journal of Electrical Power & Energy Systems*, 2023, vol. 153, article 109392.

[6] Palanimuthu, K., Joo, Y.H. Reliability improvement of the large-scale wind turbines with actuator faults using a robust fault-tolerant synergetic pitch control. *Renewable Energy*, 2023, vol. 217, p. 119164.

[7] Alemu, M., Ayenew, E. Optimal control of the electro-hydraulic actuator for variable pitch variable speed wind turbine: Performance enrichment. *Wind Engineering*, 2024.

[8] Majout, B., El Alami, H., Salime, H., Laabidine, N.Z., El Mourabit, Y., Motahhir, S., Bouderbala, M., Karim, M., Bossoufi, B. A review on popular control applications in wind energy generator PMSG. *Energies*, 2022, vol. 15, p. 6238.

[9] Baimel, D., Belikov, J., Guerrero, J.M. Dynamic modeling of networks, microgrids, and renewable sources in the dq0 reference frame: A survey. *IEEE Access*, 2017, vol. 5, pp. 21323–21335.

[10] Vu, M.T., Nguyen, V.-T., Do, Q.T., Youn, W., Nguyen, T.H. Robust non-integer predictive control for wind turbine pitch angle regulation in

full load regions using deep on-policy learning. *Engineering Applications of Artificial Intelligence*, 2025, article 111156.
[11] Ma, R., Siaw, F.L., Thio, T.H.G. A Hybrid Fuzzy LQR-PI Blade Pitch Control Scheme for Spar-Type Floating Offshore Wind Turbines. *Journal of Marine Science and Engineering*, 2024, vol. 12, no. 8, p. 1306.
[12] Dib, F., Boumhidi, I., El Akchioui, N., Benaya, N. Sliding Mode Control Optimized by Teaching Learning-Based Optimization Algorithm for Variable Speed Wind Turbine System. *2019 International Conference on Wireless Technologies, Embedded and Intelligent Systems (WITS)*, 2019, pp. 1–6.
[13] Zhou, Z., Wang, S., Jiang, J., Li, H., Zhao, J., Yu, D. Optimizing wind turbine blade pitch control via input-output model-free adaptive control. *Scientific Reports*, 2025, vol. 15, p. 6325.
[14] Mahmoud, M.M., Atia, B.S., Abdelaziz, A.Y., Nour Aldin, N.A. Dynamic performance assessment of PMSG and DFIG-based WECS with the support of manta ray foraging optimizer considering MPPT, pitch control, and FRT capability issues. *Processes*, 2022, vol. 10, no. 12, p. 2385.
[15] Nasiri, M., Mobayen, S., Zhu, Q.M. Individual pitch angle control of a variable speed wind turbine using adaptive fractional order non-singular fast terminal sliding mode control. *International Journal of Precision Engineering and Manufacturing*, 2021, vol. 22, pp. 511–522.
[16] Chavero-Navarrete, E., Trejo-Perea, M., Jáuregui-Correa, J.-C., Carrillo-Serrano, R.-V., Rios-Moreno, J.-G. Pitch angle optimization by intelligent adjusting the gains of a PI controller for small wind turbines in areas with drastic wind speed changes. *Sustainability*, 2019, vol. 11, no. 23, p. 6857.
[17] Chen, J., Yang, B., Duan, W., Shu, H., Na, A., Chen, L., Yu, T. Adaptive pitch control of variable-pitch PMSG based wind turbine. *Applied Sciences*, 2019, vol. 9, no. 19, p. 4032.
[18] Bahgat, M., Ezzat, M., Attia, M.A., Mekhamer, S.F., Elbehairy, N.M. Comparative analysis of PI and fuzzy logic controller for grid connected wind turbine under normal and fault conditions. *Scientific Reports*, 2025, vol. 15, p. 85073.
[19] Zhao, H., Ru, P., Yang, X., Xu, Y. A pitch angle controller based on novel fuzzy-PI control for wind turbine load reduction. *Energies*, 2020, vol. 13, no. 22, article 6086.
[20] Behera, S., Subudhi, B., Pati, B.B. Design of PI controller in pitch control of wind turbine: A comparison of PSO and PS algorithm. *International Journal of Renewable Energy Research*, 2016, vol. 6, no. 1.
[21] Taher, S.A., Farshadnia, M., Mozdianfard, R. Optimal gain scheduling controller design of a pitch-controlled VS-WECS using DE optimization algorithm. *Applied Soft Computing*, 2013, vol. 13, pp. 2215–2223.

Hazem Hassan Ali Sayed, Lecturer at NCT University, Egypt. Head of Energy at Luminous Energy Solutions, Energy Management Department, Canada. Research interests: energy management, renewable energy, power quality.
E-mail: hazem.hassan@nctu.edu.eg
ORCID: https://orcid.org/0000-0003-1093-853X